Noname manuscript No.
(will be inserted by the editor)

A Silicone-based Soft Matrix Nanocomposite Strain-like Sensor Fabricated using Graphene and Silly Putty ®

Marie Hébert · Jan P. Huissoon · Carolyn L. Ren

Received: date / Accepted: date

Abstract Off-the-shelf planar strain gauges are ubiquitous and are generally designed for materials with a large elastic modulus such as steel or aluminum. Correspondingly, the strain gauges themselves are stiff and do not deform substantially under applied stress. Pairs of this type of strain gauge are typically used in a Wheatstone bridge circuit allowing the measurement of very small changes in resistance due to the changes in sensing element cross-sectional area to be measured. However, their use with softer low-modulus materials is limited due to the larger elastic deformations involved. The conductive property of graphene is leveraged to produce a different type of strain sensor that is sensitive yet also capable of significant elastic deformation. The graphene is dispersed in a silicone-based polymer matrix such that the deformation induces a change in resistance that can be measured using a voltage divider circuit. The target application for which this sensor is developed is to measure strain in a pressurized length of soft Tygon® tubing which is often used in pumping fluids through microfluidic devices. However, the silicone-based graphene polymer can easily be applied to a variety of other shapes and soft materials.

Keywords Sensor · Strain gauge · Graphene · Nanocomposite · Silicone-based polymer · Tubing dynamics · Active microfluidics

Prof. Carolyn L. Ren
Mechanical and Mechatroncis Engineering at University of Waterloo,
200, University Avenue West, Waterloo, Ontario, Canada.
Tel: +1 519 888 4567 x 33030.
E-mail: c3ren@uwaterloo.ca

1 Introduction

1.1 Microfluidics context

Microfluidics deals with fluid flow at the micrometre scale. This enabling technology has been applied in a wide range of fields such as biological assays (Azizi et al. 2019), material synthesis (Wang et al. 2017), biofuels (Bodénès et al. 2019), and many more. Droplet microfluidics is a subset of microfluidics that considers monodispersed picoliter to nanoliter-sized droplets as reaction vesicles. The immiscibility of the two phases in combination with the microchannel wall surface properties allows the isolation of the dispersed phase droplets (i.e. water) within the continuous phase (i.e. oil). Hence, the chemical reactions occurring in the droplets are confined with high integrity in addition to the other main advantages of using microfluidics, namely, reduced reagent consumption and shorter reaction time.

Generally, microfluidics methods for liquid manipulation can be categorized as either passive or active. Passive approaches rely on the microchannel network geometry and arrangement to achieve the desired manipulations while active methods introduce external forces to better control the fluid. Although there exists a wide variety of methods used to drive the flow for both passive and active microfluidic solutions, syringe pumps and pressure pumps are most widely utilized.

Syringe pumps are more forgiving than pressure pumps in terms of microchip design (Glawdel and Ren 2012); however, their performance is compromised by the inherent long oscillation period in the flow (Korczyk et al. 2011). Moreover, pressure pumps respond much faster than syringe pumps when a change is requested (Kieffer et al. 2012). Pressure pumps exhibit desirable behaviour both on short and long timescales.

The fast response of pressure pumps is especially important in active control applications. In the case of an image-based closed-loop active control system for droplet manipulation in a microfluidic chip, the droplet location in a channel network is obtained from a microscope camera image. The droplet location is fed back to the controller, which adjusts the pressures applied to the channels to achieve the desired position or motion of the droplet. The required quick adjustment response of the fluid pressures can only be achieved by a pressure pump (Hébert et al. 2019). Active droplet control platforms such as this offer unique advantage for manipulating individual droplets, and present opportunities to apply microfluidics in other fields such as biochemistry for single-cell analysis.

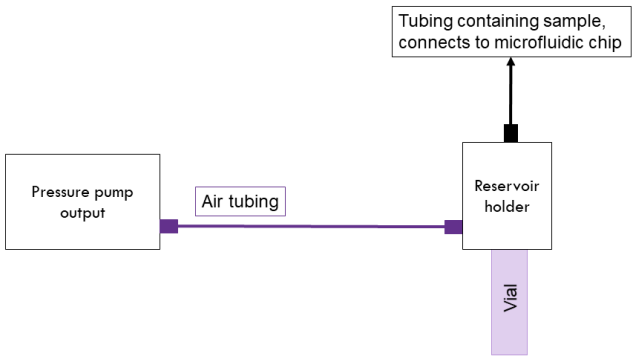

Fig. 1 Setup of the air tubing between the pressure pump and the reservoir holder.

Previous studies concerning the development of this active platform have reported somewhat limited accuracy (Wong and Ren 2016, Hébert et al. 2019). Contributing factors include image quality and pressure pump response, but the dynamic response of the tubing connecting the pressure pump and the microfluidic chip is also considered important. The impact of the tubing dynamics is that the pressure at the chip is not the same as the output pressure of the pump. Referring to Figure 1, the tubing consists of two parts: the first (air tubing) transports air from the pump to the reservoir holder; the second (liquid tubing) transports the liquid sample from the reservoir holder to the microfluidic chip. The recommended air tubing is softer than the liquid tubing, with typically an order of magnitude difference in elastic modulus. Consequently, the fluid dynamics under applied pressures in the liquid tubing can be described by the Hagen-Poiseuille law and are accounted for in the controller. However, the dynamics of the air tubing depends on its material properties and dimensions, and has not yet been accounted for in the model used for controller design. The hypothesis is that neglecting the air tubing dynamics results in lower accuracy in active control for droplet microfluidics. This, in turn, hinders the adoption of droplet microfluidics as an enabling tool for single-cell analysis, high demand in many fields such as disease diagnosis and personalized medicine (Tavakoli et al. 2019; Jin et al. 2018). To justify the efforts to evaluate and consider tubing dynamics in the active control system, it is important to quantify the impact of tubing dynamics on the performance of the active control system.

1.2 Motivation

The active control system for droplet microuidics uses droplet position feedback provided by analysis of images from a camera attached to a microscope. Together with custom software and appropriate controller parameters, the pressure to be applied at each microchip inlet is calculated multiple times per second (Wong and Ren 2016, Hébert et al. 2019). These pressures are sent to the pressure pump as commands to quickly actuate the fluid. If tubing dynamics are neglected, the set of pressures applied at the reservoir holder is assumed to be the same as the output pressures at the pump. However, in practice, both an offset and delay between the output pressures at the pump and the actual pressures applied at the reservoir holder are observed, which can cause difficulty in achieving the desired droplet manipulation. The net effect is that droplet motions must be slowed which makes the operation less efficient and longer; this is undesirable since some biochemical materials can be time-sensitive due to aggregation.

The better strategy is to account for the dynamic pressure difference, which requires an understanding of the air tubing dynamics. Tubing dynamics are influenced by multiple factors such as its inner and outer diameter, length, and stiffness. For a given material, the tubing diameter and wall thickness are the key parameters that determine the dynamic response. Incorporating changes in these parameters (or strain) as the internal pressure changes into a dynamic model should enable these effects to be compensated. The motivation is thus to develop a technique whereby the large strains encountered in the relatively soft tubing can be measured in real-time.

1.3 Literature overview

Although there exists pertinent previous research, the context and the corresponding assumptions differ sufficiently to justify investigating the specific setup of the pressurized air tubing shown in Figure 1. The two clos-

est cases in the literature are transmission lines for unsteady pressure measurement and blood flow in arteries.

A remotely localized pressure sensor requires a transmission line to measure the pressure at the location of interest. Concerns with short term variations for the measurement of unsteady pressure can be addressed by describing the dynamics of the transmission line using a 2nd order system (Doebelin and Manik 2007). However, the derivation assumes rigid walls as this is the more desirable configuration for remote pressure sensing. Therefore, such modelling would not capture the tubing compliance and its consequent dynamic effects on pressure.

Blood flow through arteries is a typical context studying the pressure propagation through compliant tubing (Čanić et al. 2006). However, once again, an assumption at the foundation of the derivations threatens the applicability to the air tubing of this study. The typical artery dimensions justify the use of thin-wall assumptions; however, the wall thickness of the air tubing herein under study is of the same order of magnitude as the inner radius. Therefore, thin-wall assumptions made for artery flow seem unreasonable.

1.4 Thick-wall compliant tubing dynamics

The dynamics introduce from the thick-wall compliant tubing between the pressure pump output and the reservoir holder are of particular importance for active control within the context of microfluidics. The available literature either does not consider the expansion of the tubing or its thick-walled properties. Hence, an experimental approach is necessary and used here. Nonetheless, the relationship between inner pressure and radial strain is established in the literature (Schmid et al. 2014).

$$\epsilon = \frac{P}{E}\left(\frac{r_o^2 + r_i^2}{r_o^2 - r_i^2} + \nu\right) \tag{1}$$

where ϵ is the radial strain [ ], P is the internal tubing pressure $[Pa]$, E is the tubing elastic modulus $[Pa]$, r_o is the outside tubing radius $[m]$, r_i is the inner tubing radius, and ν is the tubing material Poisson ratio [ ].

Typical off-the-shelf planar strain gauges are ubiquitous but are generally designed for materials with a large elastic modulus such as steel or aluminum. Correspondingly, the strain gauges themselves are stiff; they are meant to not deform substantially under applied stress. Very small changes in resistance occur due to the changes in the sensing element cross-sectional area. Pairs of this type of strain gauge are used in a Wheatstone bridge circuit to measure such small changes in resistance. However, their use with softer low modulus materials is limited due to the larger elastic deformations involved. Consequently, an alternative approach must be used. The conductive property of graphene is leveraged to produce a different type of strain sensor that is sensitive yet also capable of significant elastic deformation (Boland et al. 2016). The graphene is dispersed in a silicone-based polymer matrix such that the deformation induces a change in resistance that can be measured using a voltage divider circuit.

The strain sensor herein developed aims to measure the external radial deformation caused by the pressure within the soft tubing. The strain sensor has a silicone-based polymer matrix for its comparable softness and dispersed graphene for its current conducting properties. The deformation measurement can provide more information about the dynamics of the air tubing as it expands and contracts according to its internal pressure.

2 Materials and experimental methods

2.1 Materials

The graphene-based strain sensor can simply be fabricated with graphene, Silly Putty®, acetone, and silicone oil 5cst.

The graphene has between 5 and 10 layers, a purity of 99.5%, and a lateral size of $5 - 10\mu m$. The supplier selected for the graphene is accessible for its price range as well as ease to place an order (`https://www.ebay.ca/itm/142264483086`). The Silly Putty® is a brand by Crayola. Although its exact composition is unknown, its viscoelastic properties have previously been studied (Cross 2012). The putty is the soft matrix containing the graphene and is a silicone-based polymer. Acetone is used as the solvent for both the Silly Putty® and to disperse the graphene. The silicone oil 5cst (*Millipore Sigma*) matches the silicone-based chemistry of the Silly Putty® matrix.

Briefly, the fabrication procedure consists of dispersing the graphene and Silly Putty® in acetone in two separate containers. Sonication for 6 hours with intermittent hourly manually shaking contributes to an even dispersion within the solvent. Similarly, after combining the two acetone solutions of graphene and Silly Putty®, sonication for one hour ensures proper mixing. Afterwards, the acetone is left to evaporate at room temperature overnight. Adding a small volume (i.e. 0.1 ml) of 5cst silicone oil helps the dried mixture of Silly Putty® and graphene to regain its original texture as the final step.

Note that the dispersion of graphene within the silicone-based matrix (i.e. Silly Putty®) is named "G-putty" as per Boland et al. 2016.

2.2 Experimental setup

The G-putty is manually moulded on the tubing to give it a cylindrical shape of minimal thickness ($\sim 500\mu m$) and to establish contact with the tubing. Thus, the tubing deformation is transmitted to the G-putty. The connection to the circuit is established using small stranded wires. Although only contact is required between the wires and the G-putty to transmit the current, a more secure attachment with additional G-putty and tape is used to secure the wires on the tubing. The wires connecting the sensor to the circuit are small stranded wires to minimize interference with the deformation but maximize contact. The strain sensor cover a length of about 1.5 cm located in the middle of the tubing between the two pressure sensors. The Tygon®has a length of $\sim 50cm$, a nominal inner diameter of 1/16", and an outer diameter of 1/8".

The electrical measurement relies on a voltage divider circuit that allows to calculate the varying resistance (Z_{sensor}) based on a known precise voltage input (V_{reg}) and resistance (R_1) as per the following equation.

$$Z_{sensor} = \frac{R_1}{\frac{V_{reg}}{V_{out}} - 1} \tag{2}$$

This configuration is preferred over the more typical Wheatstone bridge circuits of strain sensors; the G-putty absolute resistance value varies and makes it difficult to match. The sensor is sensitive enough not to require a more complex circuit. The circuit overview is shown in Figure 2. Although the sensor would ideally simply behave as a resistor, an impedance is used to represent the sensor due to its more complex behaviour. The high impedance of the strain sensor ($\mathcal{O}(M\Omega)$) and the correspondingly matched resistance of the voltage divider circuit requires a voltage follower (*Texas Instrument TLC2272*) to accurately measure at the desired 1 ms interval. Moreover, an external Digital-to-Analog converter (DAC) with 12-bit resolution (*Microchip MCP3202*) and an accurate voltage reference (*Maxim Integrated MAX6250*) are set up to increase the measurement resolution. An *Arduino Mega2560* is used to communicate with the computer via serial communication.

3 Results and discussion

The pressure at one end of the soft tubing can be controlled using the pressure pump. The two pressure sensors (TE connectivity U536D-H00015-001BG) at either end of the tubing measure the pressure while the strain sensor measures the tubing radial strain caused by the tubing expansion. The specifications of the pressure sensing apparatus are given in Table 1.

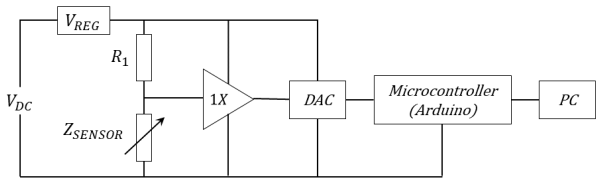

Fig. 2 Overview of the circuit: V_{DC} is the power supply voltage, V_{REG} provides a precision reference and supply voltage, $1X$ represents the voltage follower, and DAC is the digital-to-analog converter

Table 1 Specification summary for the pressure sensors (*TE Connectivity U536D-H00015-001BG*).

Range	0 to 1 bar
Accuracy	± 1 mbar
Resolution	0.24 mbar
Sampling	1 kHz

3.1 Step input

The input of the pressure pump outlet is successively increased by 100 mbar step changes. Correspondingly, the strain sensor resistance changes. However, as illustrated by Figure 3, for constant pressure and hence, constant radial strain, the strain resistance diminishes. This is attributed to the intrinsic dynamical behaviour of the nanocomposite strain sensor. The self-healing properties originate from the mobility of the graphene within the matrix (Boland et al. 2016). The dynamics can be partly explained by a transfer function with a single zero (i.e. $G(s) = s + a$). Nevertheless, the intrinsic dynamics effects clearly dominate and another approach is sought using the ramp input response.

3.2 Ramp input

The step response (Figure 3) suggests that although the strain sensor is sensitive enough to detect the small radial strain, the intrinsic dynamics introduced dominates. This is clear at constant pressure. Therefore, the ramp input response is investigated as shown in Figure 4.

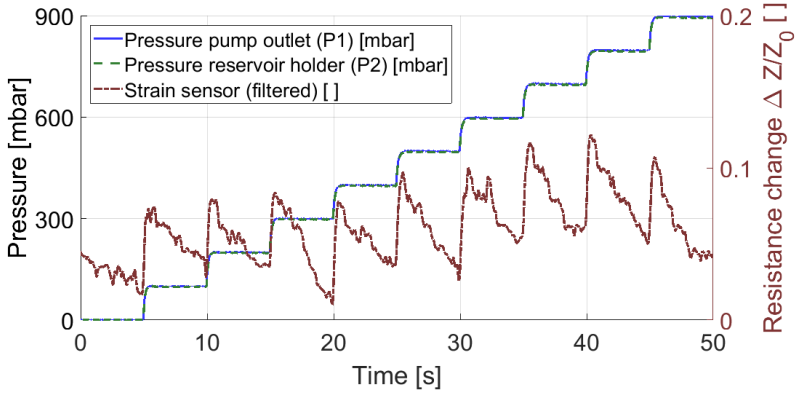

Fig. 3 Successive step input response with strain sensor measurement. The intrinsic nanocomposite strain sensor properties dominates the response at steady pressure. The sharp pressure increase and corresponding sharp change in the sensor resistance nonetheless indicates responsiveness for the small scale deformations.

Two different rates of change for the ramp are shown in Figure 4(a) and 4(b) for the milder and steeper ramp respectively. The pressure spanned is 900 mbar for both but the time required to reach this maximum pressure is 45 seconds and 9 seconds respectively. The subfigures with identical y-axis limits show a similar response trend for the strain sensor measurements.

On one hand, the step response shows that the resistance change is not significant at constant pressures; the peaks at the step change edge are all within about 5% of each other. On the other hand, the ramp response shows a significant change ($\sim$ 50%) over the same 900 mbar pressure range. Moreover, the consistency in response with respect to the rate of both the pressure and strain sensor measurement change suggests a constant relationship. However, the characterization of that constant is not done in detail here. It is hypothesized that the constant is a function of the volume ratio of graphene to Silly Putty®.

$$\frac{\partial(\Delta R/R_0)/\partial t}{\partial P/\partial t} = k, \ \textit{where } k \textit{ is a constant.} \tag{3}$$

Therefore, now revisiting the relationship between inner pressure and radial strain from Schmid et al. 2014 shown in Equation 1, the time derivative of the resistance (and hence of the strain) and the pressure time derivative are considered. However, the Silly Putty® and the tubing wall material exhibits viscoelastic behaviour. While the Silly Putty® is characterized in the literature (Cross 2012), the Tygon® tubing is not; its modulus of elasticity is about 7 MPa. Considering the tubing elastic modulus E as a function rather than a constant would affect the strain rate as part of the change with respect to time. This behaviour could be attributed to the viscoelastic properties of the material rather than to fluctuation in pressures, which is being measured. Therefore, the tubing elastic modulus (E) is considered as a constant in this study. Please note that this assumption might not be reasonable for all cases.

$$\frac{\partial \epsilon}{\partial t} = \frac{1}{E}\left(\frac{r_o^2 + r_i^2}{r_o^2 - r_i^1} + \nu\right)\frac{\partial P}{\partial t} \tag{4}$$

where ϵ is the radial strain [ ], t is time $[s]$, P is the internal tubing pressure $[Pa]$, E is the tubing elastic modulus $[Pa]$, r_o is the outside tubing radius $[m]$, r_i is the inner tubing radius, and ν is the tubing material Poisson ratio [ ].

The relationship from Equation 4 depends on the mechanical properties of the tubing to establish the proportional relationship between the pressure rate of change and the strain rate of change. The gauge factor (GF) can be estimated from the ramp response (Figure 4) by averaging the milder and steeper response. Although the data enables the estimation of the gauge factor (GF) as 20, many variables are foreseen to affect the value; the estimation should be verified for specific volume fractions, sensor geometries, and measurement resolution.

3.3 Potential impact

As previously specified, the dynamics introduced by the soft tubing in the context of active control in microfluidics is impactful. The deformation of the tubing requires special consideration of the dynamics as opposed to the simpler case of rigid-wall tubing. A strain sensor measuring deformation is particularly insightful.

The usefulness of quantifying deformation is not restricted to microfluidics but could also be extended to other areas for which traditional strain sensors can be inadequate, for example, soft robotics.

Furthermore, the development and understanding of a silicone-based soft matrix nanocomposite strain sen-

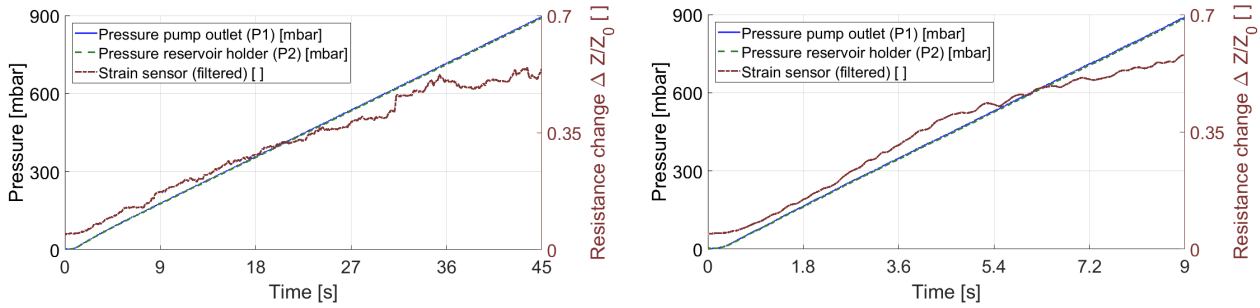

(a) Milder ramp input response strain sensor measurement. (b) Steeper ramp input response strain sensor measurement.

Fig. 4 Ramp input response. The similar response between the milder and steeper pressure ramp inputs suggests a constant relationship with the strain time derivative.

sor can be valuable for the materials field. Graphene exhibits various interesting properties that can be leveraged in different ways.

In order to further develop this silicone-based soft matrix nanocomposite strain sensor, its inherent response should be better characterized. Moreover, although the viscoelastic behaviour of Silly Putty® is reported in the literature, the impact of the graphene dispersion should be better assessed. Finally, a pole could be introduced to make an active sensor without requiring to numerically compute the derivative; hence, the response from the zero could be compensated.

4 Summary

The fast response of a pressure-driven flow setup can be leveraged in the context of an active microfluidics platform. However, although passive microfluidics can disregard any short-term dynamics and compensate for any static offset, the fast actuation of the pressure (multiple times per second) for active platforms does not allow such leniency. The compliant thick-wall tubing between the pressure pump output and the reservoir holder input is pressurized with air and introduces short-term dynamics. In order to better quantify the intrinsic dynamics of the compliant tubing, the aim is to measure its deformation using a silicone-based soft-matrix nanocomposite strain sensor (i.e. graphene dispersed in a Silly Putty® matrix: G-putty).

The strain sensor itself also introduces inherent dynamics of its own that are not well characterized. Consequently, instead of measuring the absolute value of the strain, its derivative is investigated. The ramp input response for different rates indicates that the ratio between the strain derived with respect to time and the pressure derivative are related through a constant.

Acknowledgements

The authors acknowledge the funding provided by NSERC in the form of grants supplied to Prof. Carolyn Ren and scholarships awarded to Marie Hébert.

Conflict of interest

The authors declare that they have no conflict of interest.

References

M. Azizi, M. Zaferani, S. H. Cheong, and A. Abbaspourrad. Pathogenic bacteria detection using rna-based loop-mediated isothermal-amplification-assisted nucleic acid amplification via droplet microfluidics. *ACS sensors*, 2019.

P. Bodénès, H.-Y. Wang, T.-H. Lee, H.-Y. Chen, and C.-Y. Wang. Microfluidic techniques for enhancing biofuel and biorefinery industry based on microalgae. *Biotechnology for biofuels*, 12(1):33, 2019.

C. S. Boland, U. Khan, G. Ryan, S. Barwich, R. Charifou, A. Harvey, C. Backes, Z. Li, M. S. Ferreira, M. E. Möbius, et al. Sensitive electromechanical sensors using viscoelastic graphene-polymer nanocomposites. *Science*, 354(6317):1257–1260, 2016.

S. Čanić, J. Tambača, G. Guidoboni, A. Mikelić, C. J. Hartley, and D. Rosenstrauch. Modeling viscoelastic behavior of arterial walls and their interaction with pulsatile blood flow. *SIAM Journal on Applied Mathematics*, 67(1):164–193, 2006.

R. Cross. Elastic and viscous properties of silly putty. *American Journal of Physics*, 80(10):870–875, 2012.

E. O. Doebelin and D. N. Manik. Measurement systems: application and design. 2007.

T. Glawdel and C. L. Ren. Global network design for robust operation of microfluidic droplet generators with

pressure-driven flow. *Microfluidics and nanofluidics*, 13(3):469–480, 2012.

M. Hébert, M. Courtney, and C. L. Ren. Semi-automated on-demand control of individual droplets with a sample application to a drug screening assay. *Lab on a Chip*, 19(8):1490–1501, 2019.

P. Jin, J. Lan, K. Wang, M. S. Baker, C. Huang, and E. C. Nice. Pathology, proteomics and the pathway to personalised medicine. *Expert review of proteomics*, 15(3):231–243, 2018.

C.-A. Kieffer, S. Ritty, T. Boudot, N. Petit, J. Weber, and A. Le Nel. A high-precision fluid handling system based on pressure actuation: multi-inlets flow rate control. In *Proc. 3rd Eur. Conf. Microfluidics*, volume 252, 2012.

P. M. Korczyk, O. Cybulski, S. Makulska, and P. Garstecki. Effects of unsteadiness of the rates of flow on the dynamics of formation of droplets in microfluidic systems. *Lab on a Chip*, 11(1):173–175, 2011. doi: 10.1039/c0lc00088d.

S. R. Schmid, B. J. Hamrock, and B. O. Jacobson. *Fundamentals of machine elements: SI version*. CRC Press, 2014.

H. Tavakoli, W. Zhou, L. Ma, S. Perez, A. Ibarra, F. Xu, S. Zhan, and X. Li. Recent advances in microfluidic platforms for single-cell analysis in cancer biology, diagnosis and therapy. *TrAC Trends in Analytical Chemistry*, 2019.

J. Wang, M. Jin, Y. Gong, H. Li, S. Wu, Z. Zhang, G. Zhou, L. Shui, J. C. Eijkel, and A. Van Den Berg. Continuous fabrication of microcapsules with controllable metal covered nanoparticle arrays using droplet microfluidics for localized surface plasmon resonance. *Lab on a Chip*, 17(11):1970–1979, 2017.

D. Wong and C. L. Ren. Microfluidic droplet trapping, splitting and merging with feedback controls and state space modelling. *Lab on a Chip*, 16(17): 3317–3329, 2016.

Figure 1 Setup of the air tubing between the pressure pump and the reservoir holder.

Figure 2 Overview of the circuit: V_{DC} is the power supply voltage, V_{REG} provides a precision reference and supply voltage, $1X$ represents the voltage follower, and DAC is the digital-to-analog converter

Figure 3 Successive step input response with strain sensor measurement. The intrinsic nanocomposite strain sensor properties dominate the response at steady pressure. The sharp pressure increase and corresponding sharp change in the sensor resistance nonetheless indicates responsiveness for the small scale deformations.

Figure 4 Ramp input response. The similar response between the milder and steeper pressure ramp inputs suggests a constant relationship with the strain time derivative.

Figure 4(a) Milder ramp input response strain sensor measurement.

Figure 4(b) Steeper ramp input response strain sensor measurement.